EPJ Web of Conferences **175**, 01004 (2018) https://doi.org/10.1051/epjconf/201817501004
Lattice 2017

B decay anomalies at LHCb

Arantza Oyanguren[1] (on behalf of the LHCb collaboration),*

[1] *Instituto de Física Corpuscular (IFIC), Centro mixto CSIC - Universidad de Valencia. C/. Catedrático José Beltrán, 2, 46980 Paterna, Valencia, Spain*

Abstract. The LHCb collaboration has provided a plethora of precise measurements of flavour observables in the last years. In the B meson sector some of these results show consistent deviations from Standard Model predictions with a clear tendency to specific New Physics scenarios. B decay anomalies are found in particular related to lepton flavour universality tests and angular observables in Flavour-Changing-Neutral-Current transitions. I review here the LHCb measurements and their experimental caveats. Results from Lattice are crucial in the coming years to verify if these anomalies are explained by QCD effects or if they are unambiguous hints of physics beyond the Standard Model.

1 Introduction

In the Standard Model (SM) of particle physics transitions between different quarks are governed by the Cabibbo-Kobayashi-Maskawa (CKM) mechanism [1, 2]. The amplitude of a hadron decay process can be described by using an effective weak Hamiltonian in terms of an operator product expansion (OPE), a series of effective vertices multiplied by effective couplings constants, C_i, called Wilson coefficients:

$$A(M \to F) = \langle F|\mathcal{H}_{eff}|M\rangle = \frac{G_F}{\sqrt{2}} \sum_i V^i_{CKM} C_i(\mu) \langle F|Q_i|M\rangle, \tag{1}$$

where G_F is the Fermi constant and Q_i are the relevant local operators governing the decay. The strength of the process is determined by the CKM matrix elements V^i_{CKM} and the Wilson coefficients C_i, corresponding to a given operator. These coefficients are effective couplings which depend on the arbitrary energy scale μ where short- and long- distance contributions to a given decay amplitude can be separated. The hadronic matrix elements, $\langle F|Q_i|M\rangle$, account for all QCD effects of the decay process, to be evaluated by non-perturbative methods such as Lattice QCD.

Among the six quarks which constitute the fundamental particles of the SM, the b quark is the heaviest forming hadronic bound states, the b quark having a mass around 4.7 GeV[1]. It must then necessarily decay outside the third quark family via the weak interaction, providing long lifetimes to B hadrons, of around 1.6 ps. This can be exploited by experimentalists to separate the production

* Speaker, e-mail: Arantza.Oyanguren@ific.uv.es

[1] The top quark is too heavy to hadronize.

and decay vertices of B hadrons. In addition, due to their large mass, B hadrons have many accessible decay channels with relatively small branching fractions that provide a great wealth of physics analyses.

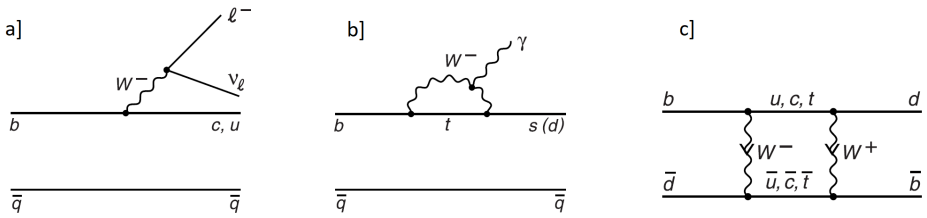

Figure 1. Tree semileptonic (a) and rare radiative (b) B hadron decays, along with B oscillation (c) diagrams.

Several types of B hadron decays can be given, some exaples are shown in Figure 1. The dominant decay processes are the tree level $b \to c$ (Cabibbo favored) and $b \to u$ (Cabibbo suppressed) transitions. Rare decays involve Flavour Changing Neutral Currents (FCNC) through quantum loops, allowing $b \to s$ and $b \to d$ transitions. In addition, B hadron decays present a pattern of flavour oscillations and CP violation. This rich phenomenology, involving quantum effects sensitive to new particles, make B decays also an ideal place for theorists to probe new physics effects.

2 The LHCb experiment

The LHCb is one of the main four detectors situated at the Large Hadron Collider (LHC) accelerator at CERN, in Geneva (Switzerland). The $b\bar{b}$ cross section in proton-proton collisions is large, around 300 (600) μb at center-of-mass-energy of 7 (13) TeV [3]. The main contribution to the b quark pair production is coming from gluon-gluon fusion. This mechanism produces b quarks back-to-back in the transverse plane. In this environment, b quarks hadronize in several species of B mesons (B, B_s, $B^{(*)}_{(s)}$) and b baryons with an average B meson momentum around 80 GeV. Since b quarks are largely produced in the forward and backward direction, the LHCb idea [4, 5] was to build a single-arm forward spectrometer covering the pseudorapidity range $2 < \eta < 5$ to study particles containing b and c quarks. The LHCb detector includes a high-precision tracking system consisting of a silicon-strip vertex detector located upstream of a 4 Tm dipole magnet, and three stations of silicon-strip detectors and straw drift tubes placed downstream of the magnet. It includes also an excellent particle identification system. Different types of charged hadrons are distinguished using information from two ring-imaging Cherenkov detectors. Photons, electrons and hadrons are identified by a calorimeter system. Muons are identified by a system composed of alternating layers of iron and multiware proportional chambers. The accuracy on the impact parameters measurement, the minimum distance of a track to a primary vertex, is about 20μm and the vertex resolution is about 15μm (70μm) in the transverse (longitudinal) planes. Figure 2 shows the layout of the LHCb detector with the different subsystems.

The LHCb experiment is at present running at high performance. An integrated luminosity of 3fb^{-1} was accumulated in Run1 at 7 TeV and 5 additional fb^{-1} are expected at 13 TeV at the end of the Run2. Figure 3 shows the integrated luminosity accumulated by the LHCb experiment during the Run1 (2011-2012) and present Run2 (2015-2017). This implies millions of b hadrons inside the LHCb acceptance. This huge amount of data allows to search for very rare B decays and perform many other physics analyses.

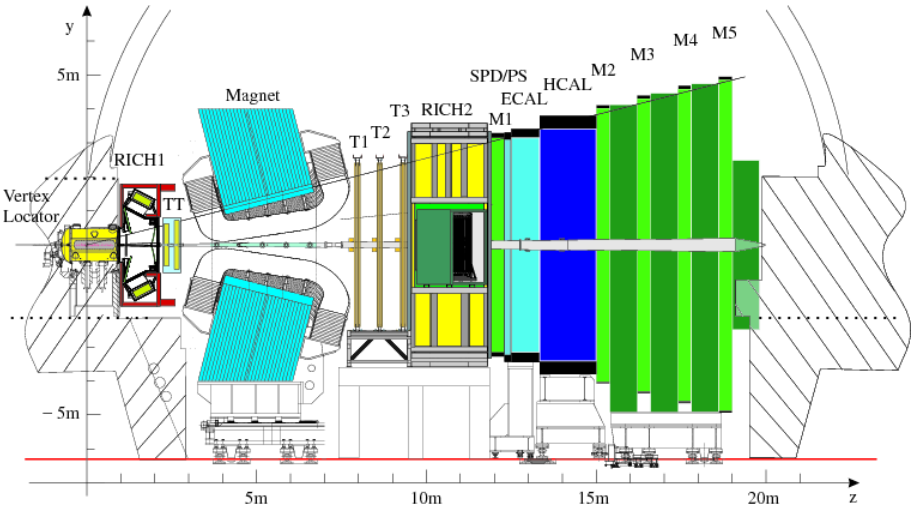

Figure 2. The LHCb detector.

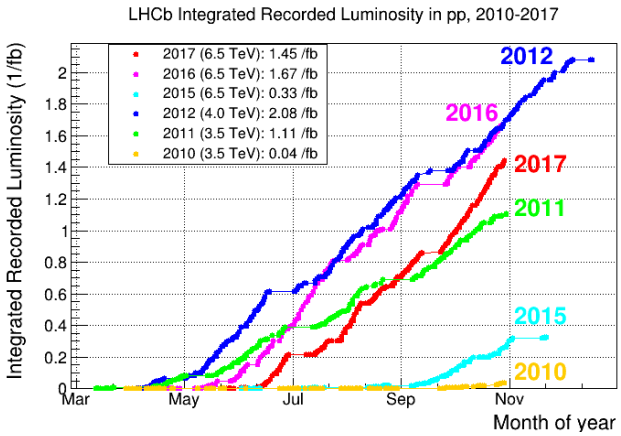

Figure 3. Integrated luminosity collected by the LHCb experiment.

3 Rare B decays

Rare $b \to s, d$ quark transitions are FCNC occurring in the SM through loops via penguin or box diagrams. Since new particles may appear in the loops they are excellent probes for physics beyond the SM. Examples of these decays are leptonic, semileptonic and radiative $b \to s$ transitions, with branching ratios ranging between 10^{-9} to 10^{-5}. Experimentally a clear signature is given by leptons or photons with high transverse momenta. Theoretically observables can be calculated in terms of Wilson coefficients as expressed in Eq. (1). All the hadronic uncertainties are embedded in decay constants or form factors and are calculated by non-perturbative methods such as Lattice QCD. Figure 4 shows as example the Feynmann diagrams for the $B_s \to \ell^+\ell^-$ transition and the corresponding decay

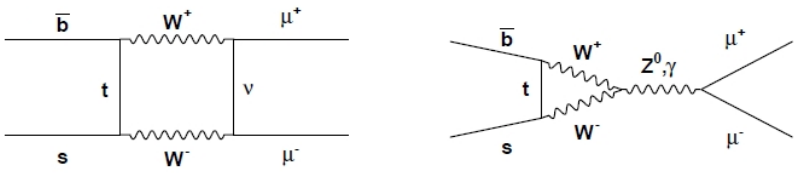

$$\Gamma\left(B_s^0 \to \mu^+\mu^-\right) \sim \frac{G_F^2\alpha^2}{64\pi^3} m_{Bs}^2 f_{Bs}^2 \left|V_{tb}V_{ts}\right|^2 \left|2m_\mu C_{10}\right|^2$$

Figure 4. Example of a rare leptonic B_s decay. The decay width of this process can be expressed in terms of the Wilson coefficient (C_{10}).

width of that process in terms of the f_{B_s} decay constant, the V_{CKM} matrix elements and the relevant Wilson coefficient, in this case C_{10}, corresponding to Q_{10}, one of the semileptonic local operators.

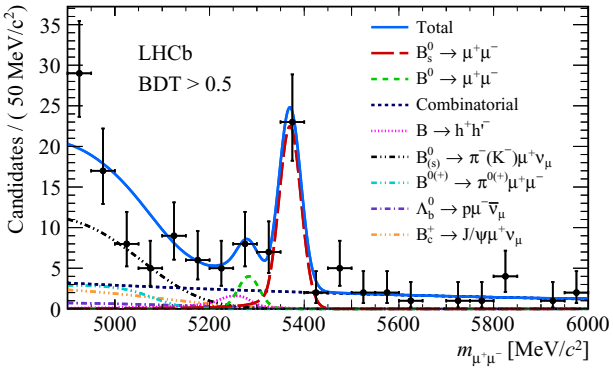

Figure 5. Mass distribution of the $B_s \to \mu^+\mu^-$ decay channel in a selected region of the BDT (Boosted Decision Tree) variable. The signal is clearly observed, the significance is 7.8σ. The $B^0 \to \mu^+\mu^-$ decay mode is also searched for. Several background components are also shown in this plot.

The $B_s \to \ell^+\ell^-$ is a very rare decay. In addition to be FCNC it is helicity suppressed and its branching fraction is predicted in the SM to be $\mathcal{B}(B_s \to \mu^+\mu^-) = (3.65 \pm 0.23) \times 10^{-9}$ [6]. This decay has been searched for over the last thirty years and was observed for first time by the LHCb and CMS experiments [7]. An updated analysis including data from Run2 has been recently performed by the LHCb experiment [8]. Results are shown in Figure 5. The measured branching fraction is $\mathcal{B}(B_s \to \mu^+\mu^-) = (3.0 \pm 0.6\,^{+0.3}_{-0.2}) \times 10^{-9}$, in agreement with the SM prediction. The theoretical uncertainties coming from the CKM matrix elements and decay constant are at present well below the statistical uncertainty, but could be improved by Lattice QCD calculations for the near future. The $B^0 \to \mu^+\mu^-$ decay mode is also searched for. No signal is found and a limit on the branching fraction $\mathcal{B}(B_s \to \mu^+\mu^-) < 3.4 \times 10^{-9}$ is set at 95% confidence level.

The $B_{(s)}$ leptonic decay channel in the tauonic mode is also searched for at LHCb [9]. The reconstruction of this mode is more complex due to the presence of at least two neutrinos originating from the τ lepton decays. No signal is found and assuming no contribution from $B^0 \to \tau^+\tau^-$ decays, the first direct upper limit on the branching fraction for the B_s channel is set to $\mathcal{B}(B_s \to \tau^+\tau^-) < 6.8\times10^{-3}$ at 95% confidence level.

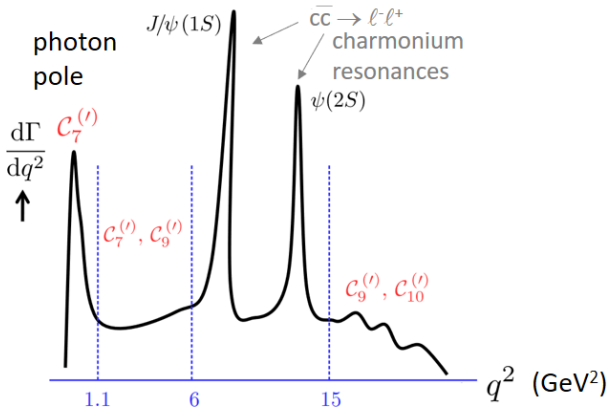

Figure 6. Differential decay width as function of q^2 for the $B \to K^{(*)}\ell^+\ell^-$ process. Each region of q^2 is sensitive to different Wilson coefficients C_i. Regions where charmonium resonances contribute are usually vetoed for the measurements. Primed coefficients correspond to right-handed currents which are suppressed in the SM.

Rare semileptonic B decays correspond to final states with two leptons and a hadron. In this case the differential branching fraction as function of q^2, the invariant mass of the two-lepton system, is measured. Each region of q^2 probes different processes and is sensitive to different Wilson coefficients as shown in Fig. 6. Regions in q^2 where charmonium resonances (J/ψ, $\psi(2S)$) are contributing are excluded from the analyses. In presence of new physics one would expect that some of the Wilson coefficients are modified from the SM value, $C_i = C_i^{SM} + C_i^{NP}$, affecting different regions of the differential decay width.

Figure 7 shows the results of several analyses performed at LHCb corresponding to the $B^+ \to K^+\mu^+\mu^-$ [15], $B_s \to \phi\mu^+\mu^-$ [16], $B^0 \to K^{*0}\mu^+\mu^-$ [17] and $\Lambda_b \to \Lambda\mu^+\mu^-$ [18] decay channels. A systematic discrepancy with the SM is observed in the region below the J/ψ resonance. The main caveat in this case is that for this observable the theory is affected by hadronic uncertainties. Form factors are evaluated by Lattice QCD at high q^2 and Light Cone Sum Rules (LCSR) at low q^2 [10–14, 19]. Non-factorisable corrections and long-distance effects could also affect the predictions.

Optimized angular observables reducing form factor dependencies have been defined [20]. The differential decay width of $B \to K^*\mu^+\mu^-$ is then described, in addition to the q^2 variable, by three decay angles: $\cos\theta_\ell$, $\cos\theta_K$ and ϕ. They are defined as the angle between the μ^+ and the direction opposite to that of the B in the rest frame of the dimuon system, the angle between the K^+ and the direction opposite to that of the B in the rest frame of the K^* system, and the angle between the plane defined by the dimuon pair and the plane defined by the kaon and pion in the B rest frame, respectively [21]. Several observables related to CP averages and CP asymmetries can be measured from the differential decay width. Measurements of this differential decay width are given by LHCb [21] ATLAS [22], Belle [23] and CMS [24]. Among these observables P_5' is expected to be theoretically

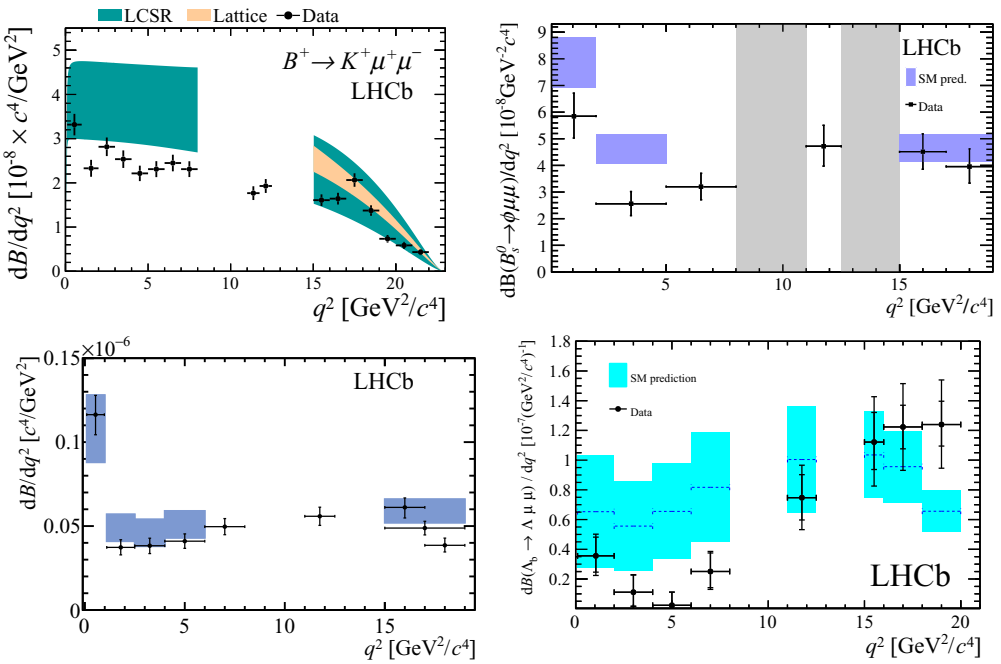

Figure 7. Differential branching fractions as function of q^2 measured by LHCb for several decay channels. Bands correspond to the SM expectations, with calculations from LQCD and LCSR [10**?** –14]

clean [20]. Figure 8 shows P_5' measured by the different experiments and compared to theoretical expectations. q^2 regions dominated by the charmonium resonances are excluded. A deviation of about 3σ from the SM prediction is observed by LHCb and confirmed by other experiments.

An explanation of this deviation from the SM could originate from long-distance contributions from the intermediate hadronic resonant states. These effects could be sizable in dimuon mass regions far from the pole masses of the J/ψ and $\psi(2S)$ resonances. Aiming at understanding long-distance contributions, the LHCb experiment has measured the phase difference between short- and long- distance amplitudes in the $B^+ \to K^+\mu^+\mu^-$ decay mode [25]. The differential decay width as function of the dimuon invariant mass is expressed in terms of form factors and Wilson coefficients, and studied across the full q^2 region. In the analysis an effective Wilson coefficient $C_9^{eff} = C_9 + \sum_j \eta_j e^{i\delta_j} A_j^{res}(q^2)$ is considered, where η_j is the magnitude of the resonance and δ_j its phase relative to C_9. The sum over j includes the ρ, w, ϕ, J/ψ and $\psi(2S)$ resonances, as well as the broad charmonium states above the open charm threshold. The amplitudes $A_j^{res}(q^2)$ are modeled using Breit-Wigner functions, and apart from the J/ψ and $\psi(2S)$ resonances, their widths and pole masses are fixed to the known values. Form factors are obtained from Lattice QCD calculations [26]. Magnitudes and phases are then extracted from data. Four degenerate solutions coming from ambiguities in the signs of the J/ψ and $\psi(2S)$ phases are obtained. Figure 9 (left) shows the solution for which both phase resonances have a negative sign. The interference with the short-distance component in dimuon mass regions far from their pole masses is found to be small. That means that the effect of hadronic resonances in the Wilson coefficients is also small. Figure 9 (right) shows the two-dimensional likelihood profile of the measured Wilson coefficients C_9 and C_{10}. The fit result deviates 3σ from the SM prediction. The dominant

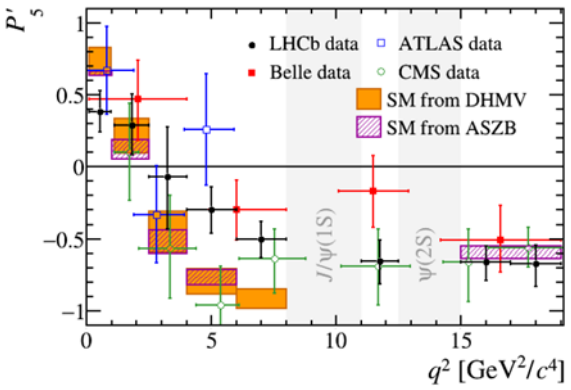

Figure 8. The optimized angular observable P'_5 measured by different experiments. Coloured bands correspond to the predictions by the SM.

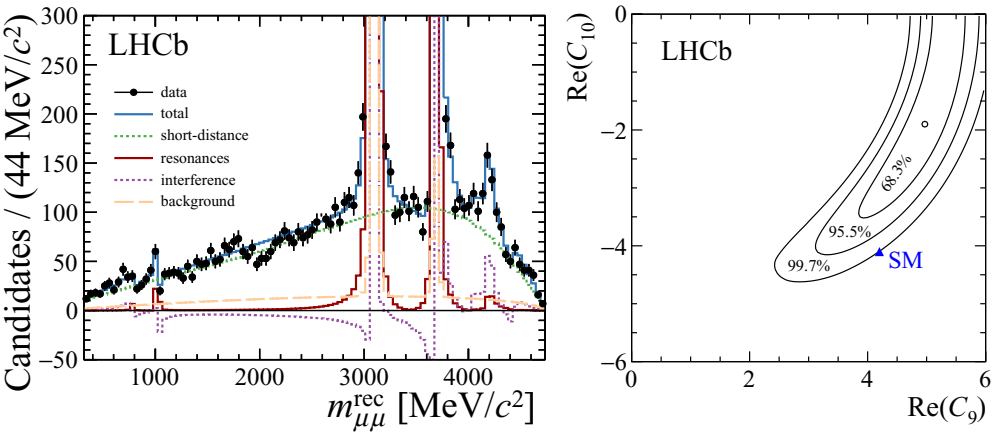

Figure 9. One of the degenerated fit solutions to the dimuon mass distribution of the $B^+ \to K^+\mu^+\mu^-$ decay channel (left) and the two-dimensional likelihood profile for the Wilson coefficients C_9 and C_{10}.

uncertainty on the C_9 and C_{10} coefficients arises from the knowledge of the B $\to$ K hadronic form factors.

Observables which are less affected by hadronic uncertainties are the rare semileptonic ratios R_H, defined as the ratio of branching fractions of a B hadron decaying in a hadron and two different species of lepton flavours, for instance $R_K = \mathcal{B}(B^+ \to K^+\mu^+\mu^-)/\mathcal{B}(B^+ \to K^+e^+e^-)$. In the SM all lepton flavours are expected to have the same couplings to gauge bosons and this ratio is one up to small corrections of order m_μ^2/m_b^2. The LHCb experiment has measured this ratio in the 1 GeV^2 < q^2 < 6 GeV^2 region [27]. Experimentally one can measure a double ratio taking benefit of the $J/\psi \to \ell^+\ell^-$ resonance. This allows to cancel many of the systematic uncertainties coming from the lepton reconstruction. In Figure 10 the q^2 distribution as a function of the invariant B^+ mass is

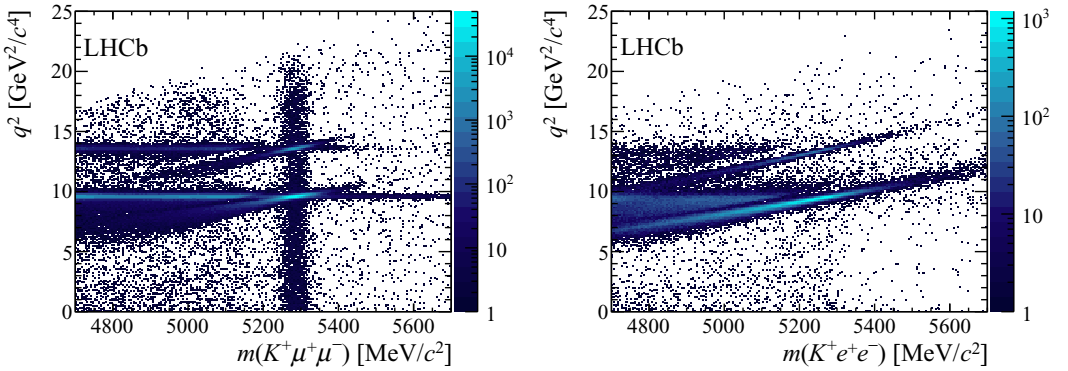

Figure 10. q^2 distribution as a function of the invariant $K^+\mu^+\mu^-$ (left) and $K^+e^+e^-$ (right) candidates.

represented for $K^+\mu^+\mu^-$ (left) and $K^+e^+e^-$ (right) candidates. For electron modes radiative emission from final state radiation and bremsstrahlung due to material in the detector have to be corrected. Due to bremsstrahlung emission the radiative tail of the J/ψ and $\psi(2S)$ is most pronounced in the electron mode. In Figure 11 (left) the fit to the mass distribution of the $K^+e^+e^-$ candidates is shown with the

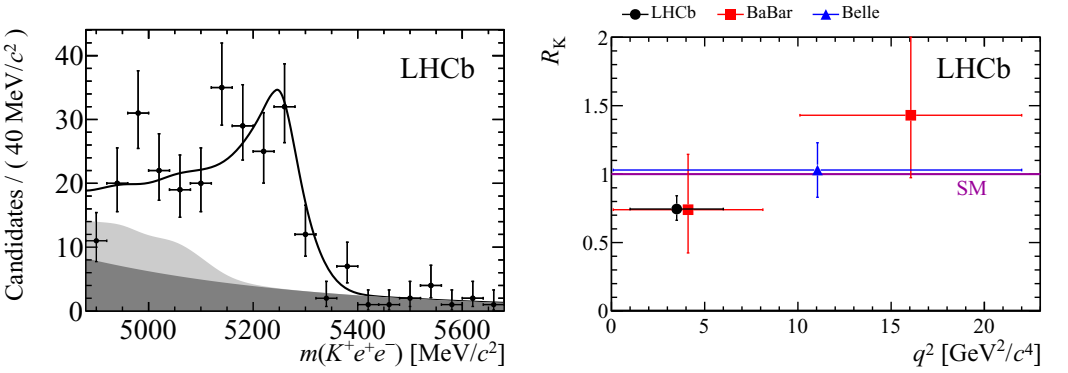

Figure 11. Left: Mass distribution of the $K^+e^+e^-$ candidates for a specific trigger category. Main backgrounds are combinatorial (dark gray) and events partially reconstructed b-hadron decays (clear gray). The fit is superimposed. Right: Comparison of the measured R_K with results from other experiments.

main backgrounds (combinatorial events and from partially reconstructed b-hadron decays) are shown in dark and clear gray respectively.

From the efficiency-corrected signal yields for the muon and electron candidates, the ratio of branching fractions is measured $R_K = 0.745\,^{+0.090}_{-0.074} \pm 0.036$, where the first uncertainty is statistical and the second one originates from systematic effects. This value is lower than the SM, at 2.6σ level. Figure 11 (right) shows the comparison of the measured R_K with results from other experiments. Theoretical uncertainties in R_K are very small due to the cancellation of form factors.

In a similar way, lepton universality has been tested at LHCb in the R_{K^*} ratio [28] with $B^0 \to K^{*0}\ell^+\ell^-$ decays. The K^{*0} is reconstructed in the final state $K^+\pi^-$ The ratio is measured in two regions

of q^2, the low-q^2 region corresponds to 0.045 GeV^2 < q^2 < 1.1 GeV^2 and the central-q^2 region, 1.1 GeV^2 < q^2 < 6 GeV^2. The SM predictions are quite precise due to cancellation of form factors: R_{K^*} = 0.922 ± 0.022 at low q^2 and R_{K^*} = 1.000 ± 0.006 at central q^2 [29–31]. Other theoretical predictions from several authors can be found in references at [28]. As in the previous analysis of R_K, the measurement is performed as a double ratio of the branching fractions of the $B^0 \to K^{*0}\ell^+\ell^-$ and $B^0 \to K^{*0}J/\psi(\to \ell^+\ell^-)$ decays to cancel systematic effects. Figure 12 shows the invariant B^0 mass distributions for electron candidates in the low (left) and central (right) q^2 regions. From the signal yields, corrected by efficiencies, the values obtained are: $R_{K^*} = 0.66\,^{+0.11}_{-0.07} \pm 0.03$ at low q^2 and $R_{K^*} = 0.69\,^{+0.11}_{-0.07} \pm 0.05$ at central q^2. The first uncertainty is statistical and the second one comes due to systematic effects. The results are compatible with the SM prediction at 2.1-2.3σ for the low-q^2 region and 2.4-2.5σ for the central-q^2 region, depending on the theoretical model used for the comparison. Figure 13 shows the comparison of the LHCb measurement with SM theoretical predictions [28].

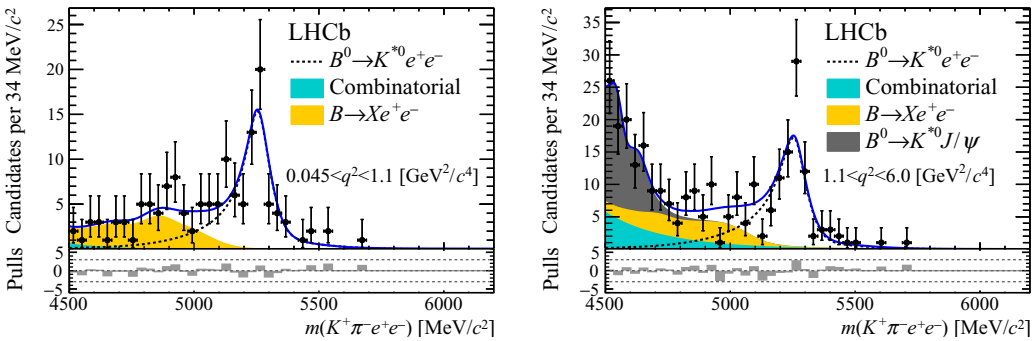

Figure 12. Mass distribution of the $K^{*0}e^+e^-$ candidates for the low-q^2 (left) and central-q^2 (right) region.

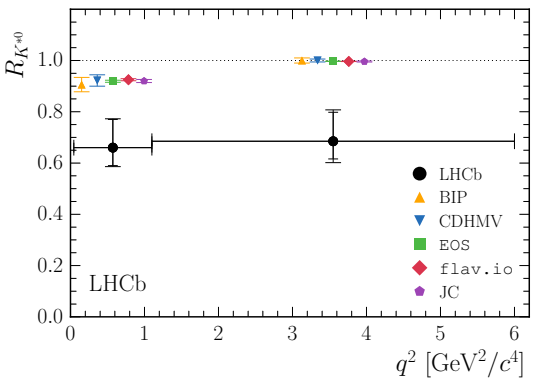

Figure 13. Comparison of the LHCb result with SM theoretical predictions. Each prediction corresponds to the same values of the low-q^2 or central-q^2 bins, they are displaced for presentation.

At LHCb, electrons are harder to reconstruct than muons at the trigger, reconstruction, selection and particle identification level. The mass resolutions of B hadron candidates with electrons are affected by bremsstrahlung and need an energy recovery treatment. To asses the procedure, analyses are performed using different independent hardware trigger categories, and the mass shape is modeled according to the number of bremsstrahlung electrons recovered. $B^0 \to K^{*0} J/\psi(\to \ell^+\ell^-)$ and $B^0 \to K^{*0}\gamma(\to \ell^+\ell^-)$ decay modes are used to control these effects. Data and simulations used in the analyses agree well and show a good performance of the technical procedures. Several cross-checks are performed to control efficiency calculations and differences between data and simulations are included in the systematic uncertainties.

Rare $b \to s$ decays can also occur with a photon in the final state (see Fig. 1 b). Even if photons are difficult to reconstruct, the LHCb experiment has measured the ratio of branching fractions $\mathcal{B}(B^0 \to K^{*0}\gamma)/\mathcal{B}(B_s \to \phi\gamma)$ with partial statistics of the Run1 [32]. The result is:

$$\frac{\mathcal{B}(B^0 \to K^{*0}\gamma)}{\mathcal{B}(B_s \to \phi\gamma)} = 1.23 \pm 0.06 \pm 0.04 \pm 0.10, \tag{2}$$

where the first uncertainty is statistics, the second systematic and the third uncertainty comes from external inputs, due to the uncertainty in hadronization fractions f_s/f_d.

A measurement of the time dependent distribution of the $B_s \to \phi\gamma$ decay channel has recently been performed [33]. This observable is sensitive to the photon polarization, which is predicted to be right-handed in $\bar{b} \to \bar{s}\gamma$ in the SM. The analysis uses the $B^0 \to K^{*0}\gamma$ decay mode as control channel. Since both mesons, the $\phi \to K^+K^-$ and the $K^{*0} \to K^+\pi^-$ decay into two charged hadrons, and the K^{*0} decay is flavour specific (no effect from new physics is expected), the $B^0 \to K^{*0}\gamma$ decay channel can be used to control reconstruction effects. Figure 14 shows the mass distribution of the $B^0 \to K^{*0}\gamma$

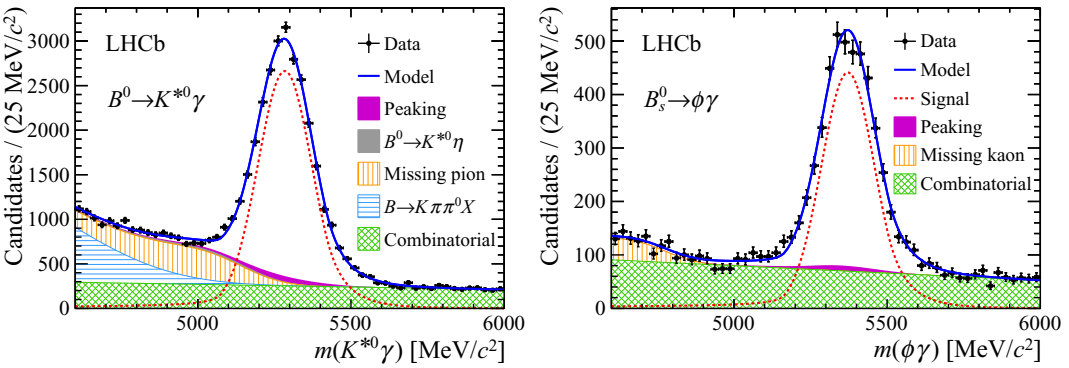

Figure 14. Mass distribution of the $B^0 \to K^{*0}\gamma$ (left) and $B_s \to \phi\gamma$ (right) candidates.

and $B_s \to \phi\gamma$ candidates. The time dependent decay width of the $B_s \to \phi\gamma$ decay channel depends on the $\mathcal{A}^\Delta$ parameter, which is related to the ratio of right and left handed amplitudes of the photon polarization. The SM prediction for this parameter is $\mathcal{A}^\Delta = 0.047^{+0.029}_{-0.025}$ [34]. This is the first time the photon polarization is studied in the B_s system. The result is $\mathcal{A}^\Delta = -0.98^{+0.46\,+0.23}_{-0.52\,-0.20}$, which is compatible with the SM within 2σ.

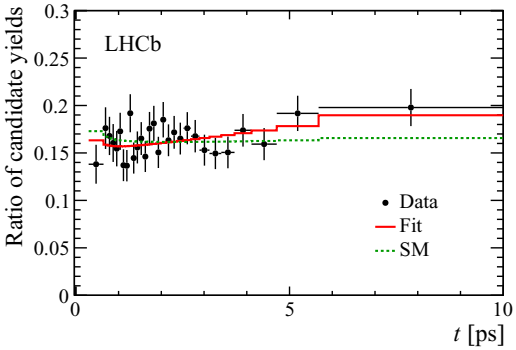

Figure 15. Fit to the ratio of the time dependent distributions for $B^0 \to K^{*0}\gamma$ and $B_s \to \phi\gamma$ signal candidates.

Figure 15 shows the result of the ratio of the decay time distributions for the $B^0 \to K^{*0}\gamma$ and $B_s \to \phi\gamma$ signal candidates after background subtraction. The SM model prediction and the result of the fit on data is presented.

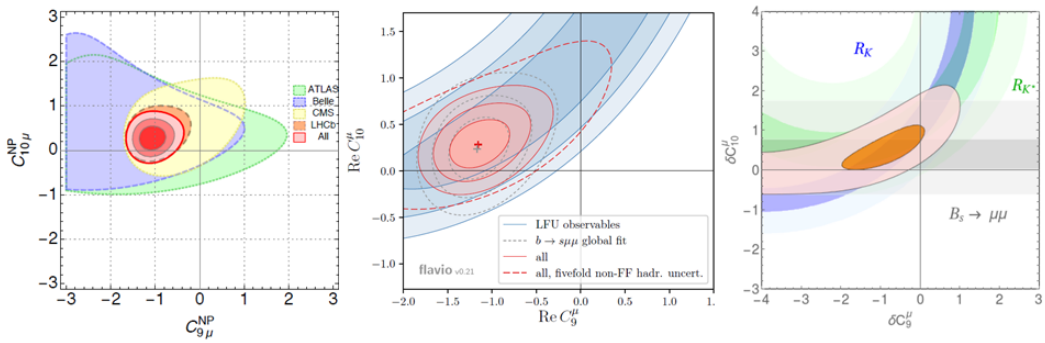

Figure 16. Results of the new physics contributions to the Wilson coefficients C_9 and C_{10} as obtained from several authors (references in the text).

In recent years the LHCb collaboration has observed tensions (at 2-3σ level) with respect to SM predictions in several rare $b \to s$ transitions. Since these observables can be expressed in terms of the Wilson coefficients as shown in Eq. (1), global fits are performed by several authors to extract possible new physics contributions. Some of these analyses include more than a hundred observables from different experiments. Figure 16 shows the results of the new physics contributions to the Wilson coefficients C_9 and C_{10} as obtained from several authors [35–37]. Details of the analyses and treatment of theoretical uncertainties can be found in the references. The new physics hypothesis is preferred over SM with a significance of about 4-5σ. The main effect is observed on the C_9 coefficient related to muons. The SM prediction is 4.27, while a shift of -1.1 to this coefficient is needed to fit the data. These results have triggered a set of models with intermediate Z', leptoquarks (LQ) and composite Higgs models.

4 Semileptonic B decays

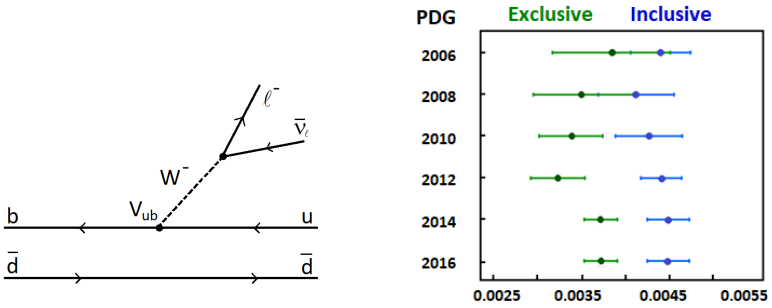

Figure 17. Feynman diagram of the Cabibbo-suppressed semileptonic B decay transition $b \to u$ (left) and evolution of the measurement of the CKM matrix elements V_{ub} with time using exclusive and inclusive decays, from the Particle Data Group.

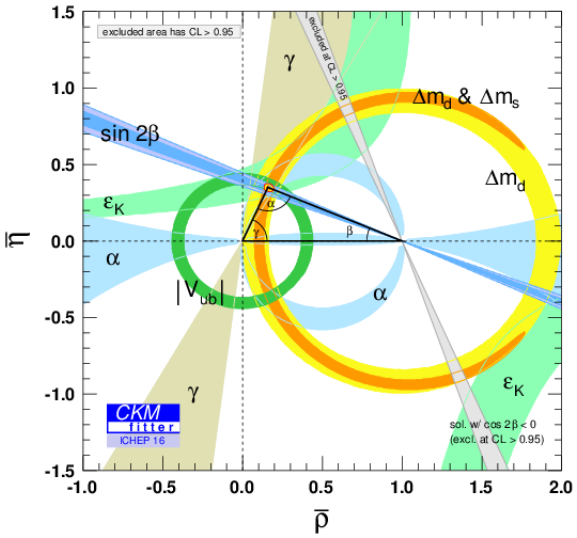

Figure 18. Left: Flavour constraints on the $\bar{\eta}$ and $\bar{\rho}$ plane from CKM fitter group). The CKM matrix element V_{ub} constraint the upper vertex of the Unitarity Triangle.

.

The $b \to c, u$ quark transitions proceed at tree level (see Fig. 17, left). The CKM matrix element V_{ub} governing the Cabibbo-suppresed process is the smallest CKM element, about 0.004. This element is crucial in constraining the flavour picture since new physics is not expected to contribute at tree level. Figure 18 shows the flavour constraints given by this CKM matrix element. The evolution

of the measurement of V_{ub} with time during the last ten years is shown in Figure 17 (right). A long-standing discrepancy of about 3σ between its determination through exclusive and inclusive decays remains still unsolved.

Aiming at contributing to solve this puzzle the LHCb experiment has measured the V_{ub} matrix element using b baryon decays for first time [38]. The ratio of branching fractions $\mathcal{B}(\Lambda_b^0 \to p\mu^-\overline{\nu}_\mu)/\mathcal{B}(\Lambda_b^0 \to \Lambda_c^+\mu^-\overline{\nu}_\mu)$ depends on the ratio of the CKM matrix elements $|V_{ub}|^2/|V_{cb}|^2$ times the ratio of the $\Lambda_b^0 \to p$ and $\Lambda_b^0 \to \Lambda_c^+$ form factors. The later have been calculated with high accuracy by Lattice QCD [39]. Using information of the primary decay vertex and the transverse momentum of the proton and muon system, signal $\Lambda_b^0 \to p\mu^-\overline{\nu}_\mu$ and $\Lambda_b^0 \to \Lambda_c^+\mu^-\overline{\nu}_\mu$ candidates are selected. Figure 19 (left) shows the corrected $p\mu^-$ mass defined as $m_{corr} = \sqrt{m_{p\mu}^2 + p_\perp^2} + p_\perp$, where $p_\perp$ is the transverse momentum of the $p\mu^-$ system. Signal and background candidates are shown. The result of the ratio of the CKM matrix elements gives:

$$\frac{|V_{ub}|}{|V_{cb}|} = 0.083 \pm 0.004 \pm 0.004, \tag{3}$$

where the first uncertainty is of statistical origin and the second one is coming from Lattice QCD calculations. Figure 19 (right) shows the result of this ratio compared to other results of the CKM matrix elements V_{cb} and V_{ub} obtained from exclusive and inclusive semileptonic decays.

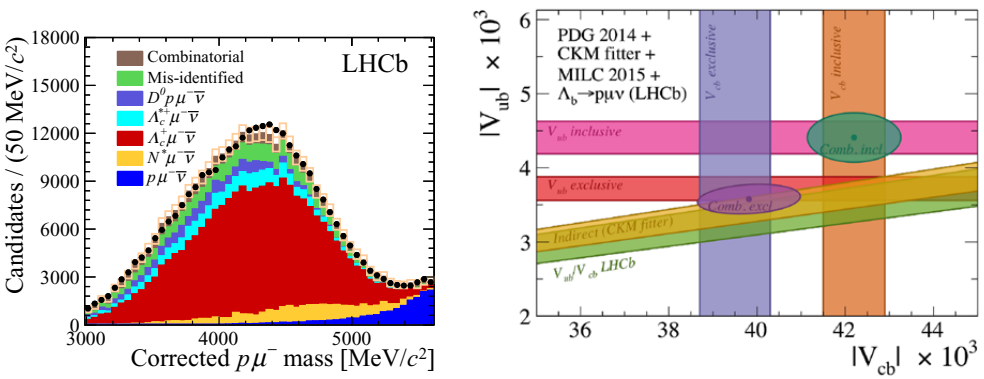

Figure 19. Corrected mass for the $p\mu$ candidates (left). Results of the measured $|V_{ub}|/|V_{cb}|$ ratio at LHCb through b baryon decays compared to other results.

Lepton flavour universality can also be tested at tree level by measuring the ratio of semi-tauonic and semi-muonic branching fractions,

$$\mathcal{R}(\mathrm{D}^{(*)}) = \frac{\overline{\mathrm{B}}^0 \to \mathrm{D}^{(*)+}\tau^-\overline{\nu}_\tau}{\overline{\mathrm{B}}^0 \to \mathrm{D}^{(*)+}\mu^-\overline{\nu}_\mu}. \tag{4}$$

The SM prediction of these ratios is very precise due to the cancellation of the CKM matrix element V_{cb} and some form factors [40–42]:

$$\mathcal{R}(\mathrm{D})_{SM} = 0.299 \pm 0.003; \qquad \mathcal{R}(\mathrm{D}^*)_{SM} = 0.252 \pm 0.003.$$

Deviations from these values could indicate new physics contributions at tree level mediated by charged Higgs bosons or leptoquarks.

The BaBar experiment has measured an excess of $\overline{B}^0 \to D^{(*)+}\tau^-\overline{\nu}_\tau$ decays [43, 44], about 3σ away from the SM predictions. The LHCb experiment has also measured $\mathcal{R}(D^*)$ using two different analyses and decay channels: $\overline{B}^0 \to D^{(*)+}\tau^-\overline{\nu}_\tau$, with the τ decaying in the channel $\tau^- \to \mu^-\overline{\nu}_\mu\nu_\tau$ [45], and the $B^0 \to D^{(*)-}\tau^+\nu_\tau$, with the τ decaying in three prongs: $\tau^+ \to \pi^+\pi^-\pi^+(\pi^0)\overline{\nu}_\tau$ [46]. In the first analysis the missing mass squared, defined as $m^2_{miss} = (P_B - P_{D^*} - P_\mu)^2$, with P_i the four-momentum of the i particle, and the muon energy, are studied in several q^2 bins. A three-dimensional fit is performed, with templates extracted from simulated samples and validated on data-driven control samples. Figure 20 (left) shows the missing mass distribution projection with the signal contribution and the different background composition. The result of the fit gives

$$\mathcal{R}(D^*) = 0.336 \pm 0.027 \pm 0.030, \tag{5}$$

where the first uncertainty is statistical and the second originates from systematic effects.

In the second analysis, the τ lepton is reconstructed in the decay mode $\tau^+ \to \pi^+\pi^-\pi^+(\pi^0)\overline{\nu}_\tau$. The measured ratio is normalized to $B^0 \to D^{*-}\pi^+\pi^-\pi^+$ to cancel systematic uncertainties coming from reconstruction efficiencies. $\mathcal{R}(D^*)$ is then obtained using the external branching fractions of the hadronic B^0 mode and of the semi-muonic decay mode. Information related to the position of the three-pion vertex is used to perform a three-dimensional fit on q^2, the decay time of the three-pion system and the response of a BDT. The result of the fit gives

$$\mathcal{R}(D^*) = 0.286 \pm 0.019 \pm 0.025 \pm 0.021, \tag{6}$$

where the first uncertainty is statistical, the second systematic, and the third is coming from the uncertainties on the external branching fractions.

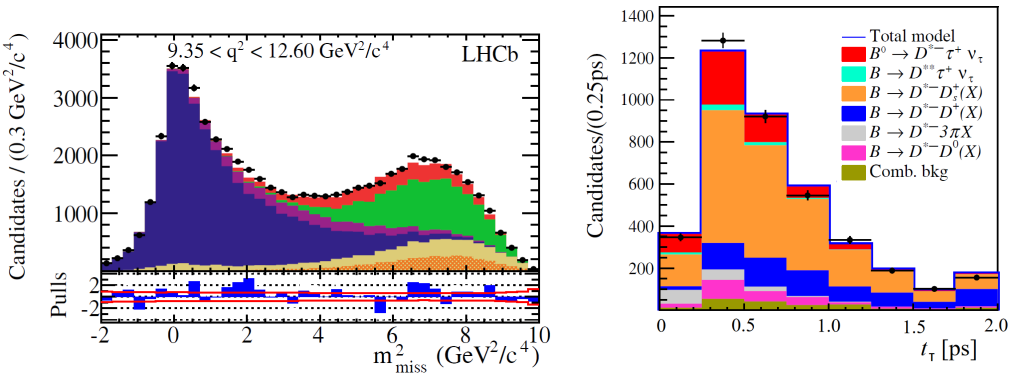

Figure 20. Missing mass squared distribution projection for the $\tau^- \to \mu^-\overline{\nu}_\mu\nu_\tau$ analysis (left) and decay time distribution projection for the $\tau^+ \to \pi^+\pi^-\pi^+(\pi^0)\overline{\nu}_\tau$ analysis (right). B semitauonic signal candidates are shown in red in both distributions. Several background contributions are also shown.

Figure 21 shows the global picture of $\mathcal{R}(D)$ and $\mathcal{R}(D^*)$ including other recent experimental results from Belle. The combined result by the HFLAV shows a deviation of about 4σ with the SM prediction.

5 Wish list for lattice

Lattice QCD inputs are decisive to solve some long-standing puzzles and to understand if B decay anomalies originate from new physics contributions or from hadronic effects. As an example, it has

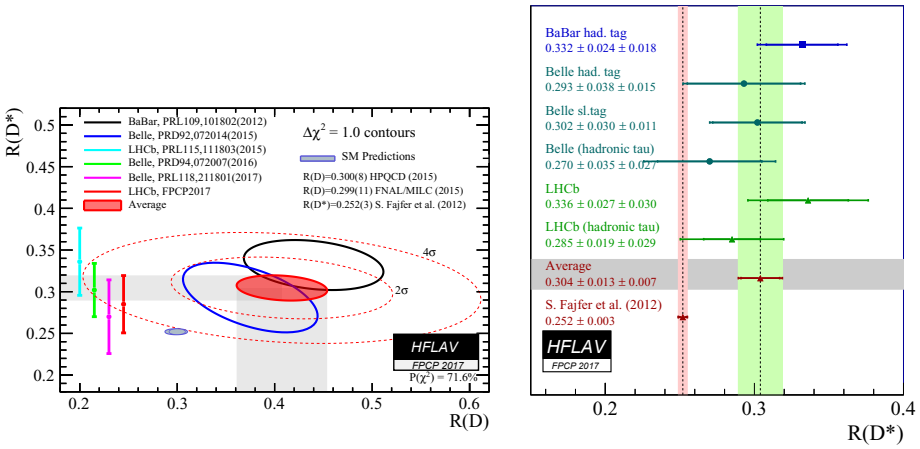

Figure 21. Combined results by HFLAV of $\mathcal{R}(D^*)$ and $\mathcal{R}(D)$ (left) and results for $\mathcal{R}(D^*)$ by several experiments. The SM prediction is also shown.

been argued [40, 47, 48] that the large difference between the V_{cb} inclusive and exclusive determinations is coming from the form factor parametrization. Understanding these differences is also relevant for the $\mathcal{R}(D^{(*)})$ determination.

My wish list for Lattice QCD to compute is:

- $B \to D^{(*)}$ form factors, affecting V_{cb} and $\mathcal{R}(D^{(*)})$, at different q^2 values.
- Other form factors (for B_s, B_c and Λ_b decays) to perform semitauonic over semileptonic rates. It would be also convenient to have $\Lambda_b \to p$ form factors computed from other groups.
- V_{cb} and V_{ub}, they are inputs for branching ratio calculation in many rare decays.
- $B_{(s)}$ decay constant, even if at present the $B_s \to \mu^+\mu^-$ branching ratio is limited by experimental (statistical) uncertainties, it will be a key observable in the coming years to confirm new physics scenarios. Other Lattice inputs going into CKM fits (matrix elements, etc...) are going to quickly become very relevant.
- $B \to K^{(*)}$ form factors, understanding of the effect from unstable resonances in form factor predictions. It would be also interesting to have form factors for higher states.
- Charm contributions in $b \to s\ell^+\ell^-$ transitions, maybe above the open-charm threshold, to be checked against data. Could Lattice do anything for the long-distance and non-factorisable corrections?
- Ratios of form factors from Lattice could help to cancel systematic uncertainties (e.g. $B \to \pi\mu^+\mu^-$ over $B \to K\mu^+\mu^-$, or $B_s \to K^*\mu^+\mu^-$ over $B \to K^*\mu^+\mu^-$).

6 Conclusions

Deviations from the SM have been found in the flavour sector by LHCb and other experiments. Discrepancies with theoretical predictions are observed in differential branching fractions ($B^0 \to$

$K^{*0}\mu^+\mu^-$, $B^+ \to K^{(*)+}\mu^+\mu^-$, $B_s \to \phi\mu^+\mu^-$, $B^+ \to \pi^+\mu^+\mu^-$ and $\Lambda_b \to \Lambda\mu^+\mu^-$), angular analyses ($B^0 \to K^{*0}\mu^+\mu^-$, $B_s \to \phi\mu^+\mu^-$, $B^0 \to K^{*0}e^+e^-$ and $\Lambda_b \to \Lambda\mu^+\mu^-$), and tests of lepton flavour universality ($B^+ \to K^+\ell^+\ell^-$, $B^0 \to K^{*0}\ell^+\ell^-$ and $B \to D^{(*)}\tau\nu_\tau$). The first type of observables could be affected by hadronic uncertainties but tests of lepton flavour universality are very clean, since hadronic uncertainties are expected to cancel in the ratios.

These deviations show a consistent pattern in global fit analyses, pointing to new physics in the Wilson coefficient C_9 and affecting differently to lepton families. They are hard to be explained just by either experimental effects or by QCD effects. But time is a great thickener of things, and with the Run2 in progress, the LHCb upgrade nextly, and Belle II just about to start, we will know soon if these new physics scenarios are confirmed.

References

[1] M. Kobayashi, T. Maskawa, Prog. Theor. Phys. **49**, 652 (1973)
[2] N. Cabibbo, Phys. Rev. Lett. **10**, 531 (1963), [,648(1963)]
[3] R. Aaij et al. (LHCb), Phys. Rev. Lett. **118**, 052002 (2017), [Erratum: Phys. Rev. Lett.119,no.16,169901(2017)], 1612.05140
[4] A.A. Alves, Jr. et al. (LHCb), JINST **3**, S08005 (2008)
[5] R. Aaij et al. (LHCb), Int. J. Mod. Phys. **A30**, 1530022 (2015), 1412.6352
[6] C. Bobeth, M. Gorbahn, T. Hermann, M. Misiak, E. Stamou, M. Steinhauser, Phys. Rev. Lett. **112**, 101801 (2014), 1311.0903
[7] V. Khachatryan et al. (LHCb, CMS), Nature **522**, 68 (2015), 1411.4413
[8] R. Aaij et al. (LHCb), Phys. Rev. Lett. **118**, 191801 (2017), 1703.05747
[9] R. Aaij et al. (LHCb), Phys. Rev. Lett. **118**, 251802 (2017), 1703.02508
[10] P. Ball, R. Zwicky, Phys. Rev. **D71**, 014015 (2005), hep-ph/0406232
[11] C. Bouchard, G.P. Lepage, C. Monahan, H. Na, J. Shigemitsu (HPQCD), Phys. Rev. Lett. **111**, 162002 (2013), [Erratum: Phys. Rev. Lett.112,no.14,149902(2014)], 1306.0434
[12] A. Bharucha, D.M. Straub, R. Zwicky, JHEP **08**, 098 (2016), 1503.05534
[13] R.R. Horgan, Z. Liu, S. Meinel, M. Wingate, Phys. Rev. **D89**, 094501 (2014), 1310.3722
[14] R.R. Horgan, Z. Liu, S. Meinel, M. Wingate, PoS **LATTICE2014**, 372 (2015), 1501.00367
[15] R. Aaij et al. (LHCb), JHEP **06**, 133 (2014), 1403.8044
[16] R. Aaij et al. (LHCb), JHEP **09**, 179 (2015), 1506.08777
[17] R. Aaij et al. (LHCb), JHEP **11**, 047 (2016), 1606.04731
[18] R. Aaij et al. (LHCb), JHEP **06**, 115 (2015), 1503.07138
[19] W. Detmold, C.J.D. Lin, S. Meinel, M. Wingate, Phys. Rev. **D87**, 074502 (2013), 1212.4827
[20] S. Descotes-Genon, T. Hurth, J. Matias, J. Virto, JHEP **05**, 137 (2013), 1303.5794
[21] R. Aaij et al. (LHCb), JHEP **02**, 104 (2016), 1512.04442
[22] T.A. collaboration (ATLAS) (2017)
[23] S. Wehle et al. (Belle), Phys. Rev. Lett. **118**, 111801 (2017), 1612.05014
[24] C. Collaboration (CMS) (2017)
[25] R. Aaij et al. (LHCb), Eur. Phys. J. **C77**, 161 (2017), 1612.06764
[26] J.A. Bailey et al., Phys. Rev. **D93**, 025026 (2016), 1509.06235
[27] R. Aaij et al. (LHCb), Phys. Rev. Lett. **113**, 151601 (2014), 1406.6482
[28] R. Aaij et al. (LHCb), JHEP **08**, 055 (2017), 1705.05802
[29] S. Descotes-Genon, L. Hofer, J. Matias, J. Virto, JHEP **06**, 092 (2016), 1510.04239
[30] B. Capdevila, S. Descotes-Genon, J. Matias, J. Virto, JHEP **10**, 075 (2016), 1605.03156
[31] B. Capdevila, S. Descotes-Genon, L. Hofer, J. Matias, JHEP **04**, 016 (2017), 1701.08672
[32] R. Aaij et al. (LHCb), Nucl. Phys. **B867**, 1 (2013), 1209.0313
[33] R. Aaij et al. (LHCb), Phys. Rev. Lett. **118**, 021801 (2017), [Addendum: Phys. Rev. Lett.118,no.10,109901(2017)], 1609.02032
[34] F. Muheim, Y. Xie, R. Zwicky, Phys. Lett. **B664**, 174 (2008), 0802.0876
[35] B. Capdevila, A. Crivellin, S. Descotes-Genon, J. Matias, J. Virto (2017), 1704.05340
[36] W. Altmannshofer, P. Stangl, D.M. Straub, Phys. Rev. **D96**, 055008 (2017), 1704.05435
[37] L.S. Geng, B. Grinstein, S. Jäger, J. Martin Camalich, X.L. Ren, R.X. Shi (2017), 1704.05446
[38] R. Aaij et al. (LHCb), Nature Phys. **11**, 743 (2015), 1504.01568
[39] W. Detmold, C. Lehner, S. Meinel, Phys. Rev. **D92**, 034503 (2015), 1503.01421

[40] D. Bigi, P. Gambino, Phys. Rev. **D94**, 094008 (2016), 1606.08030
[41] H. Na, C.M. Bouchard, G.P. Lepage, C. Monahan, J. Shigemitsu (HPQCD), Phys. Rev. **D92**, 054510 (2015), [Erratum: Phys. Rev.D93,no.11,119906(2016)], 1505.03925
[42] S. Fajfer, J.F. Kamenik, I. Nisandzic, Phys. Rev. **D85**, 094025 (2012), 1203.2654
[43] J.P. Lees et al. (BaBar), Phys. Rev. **D88**, 072012 (2013), 1303.0571
[44] G. Ciezarek, M. Franco Sevilla, B. Hamilton, R. Kowalewski, T. Kuhr, V. Lüth, Y. Sato, Nature **546**, 227 (2017), 1703.01766
[45] R. Aaij et al. (LHCb), Phys. Rev. Lett. **115**, 111803 (2015), [Erratum: Phys. Rev. Lett.115,no.15,159901(2015)], 1506.08614
[46] R. Aaij et al. (LHCb) (2017), 1708.08856
[47] D. Bigi, P. Gambino, S. Schacht, Phys. Lett. **B769**, 441 (2017), 1703.06124
[48] B. Grinstein, A. Kobach, Phys. Lett. **B771**, 359 (2017), 1703.08170